Available online at www.sciencedirect.com
SCIENCE DIRECT®
Journal of Magnetic Resonance 169 (2004) 342–350
JMR Journal of Magnetic Resonance
www.elsevier.com/locate/jmr

High resolution heteronuclear correlation NMR spectroscopy between quadrupolar nuclei and protons in the solid state

A. Goldbourt, E. Vinogradov,[1] G. Goobes,[2] and S. Vega*

Department of Chemical Physics, Weizmann Institute of Science, Rehovot, 76100, Israel

Received 22 March 2004; revised 7 May 2004
Available online 19 June 2004

Abstract

A high resolution two-dimensional solid state NMR experiment is presented that correlates half-integer quadrupolar spins with protons. In this experiment the quadrupolar nuclei evolve during t_1 under a split-t1, FAM-enhanced MQMAS pulse scheme. After each t_1 period ending at the MQMAS echo position, single quantum magnetization is transferred, via a cross polarization process in the mixing time, from the quadrupolar nuclei to the protons. High-resolution proton signals are then detected in the t_2 time domain during *w*PMLG5* homonuclear decoupling. The experiment has been demonstrated on a powder sample of sodium citrate and ^{23}Na–^{1}H 2D correlation spectra have been obtained. From the HETCOR spectra and the regular MQMAS spectrum, the three crystallographically inequivalent Na^+ sites in the asymmetric unit were assigned. This MQMAS-*w*PMLG HETCOR pulse sequence can be used for spectral editing of half-integer quadrupolar nuclei coupled to protons.

Keywords: Solid state NMR; MQMAS; Half-integer quadrupolar nuclei; High-resolution proton NMR; PMLG; *w*PMLG; FAM pulses; HETCOR

1. Introduction

The recent emergence of sensitivity enhancement and spectral resolution radiofrequency (RF) pulse schemes in solid state NMR has promoted it to a valuable tool for resonance assignment and structural characterization of solid samples in either polycrystalline or amorphic state. Consequently, high resolution NMR spectroscopy of solids has been finding its applications in several fields, ranging from polymer science [1] to biological macromolecules [2–5]. The most common nuclei observed in solid state NMR are ^{13}C, ^{15}N, ^{31}P, and ^{29}Si, all having a spin quantum number of a half, and ^{23}Na, ^{11}B, ^{27}Al, and ^{17}O, having half-integer spin quantum numbers larger than a half and thus possessing a quadrupolar interaction [6]. Sensitivity and resolution enhancement of the spectra of these nuclei are nowadays achieved with the combination of magic angle spinning (MAS) [7,8], heteronulcear dipolar decoupling [9–11], cross-polarization (CP) [12–14], homonuclear decoupling [15], and for half-integer quadrupolar spins, multiple-quantum magic angle spinning (MQMAS) [16], and satellite transition magic angle spinning (STMAS) [17]. All these techniques, aimed at achieving resolution enhancement of the NMR spectra of solids, involve the elimination of the various anisotropic spin interactions that are present in powder samples in the solid-state. Those elimination schemes are based on either spatial or spin space averaging of the undesired interactions: mechanical manipulation of the samples resulting in spatial averaging and application of RF irradiation sequences, e.g., heteronuclear dipolar decoupling, causing spin state averaging [18,19].

The most sensitive nucleus in liquid state NMR, having a spin-1/2, is ^{1}H. In solid state NMR the detection

* Corresponding author. Fax: +972-8-934-4123.
E-mail address: shimon.vega@weizmann.ac.il (S. Vega).
[1] Present address: Department of Radiology, Beth Israel Deaconess Medical Center, One Deaconess Road, Boston, MA 02215, USA.
[2] Present address: Department of Chemistry, Box 351700, University of Washington, Seattle, WA 98195, USA.

1090-7807/$ - see front matter © 2004 Elsevier Inc. All rights reserved.
doi:10.1016/j.jmr.2004.05.013

of proton spectra is difficult due to dominating strong homonuclear dipolar couplings, resulting in broad and featureless spectral lines. The acquisition of high resolution solid state proton spectra is presently accomplished by combining MAS and RF irradiation pulse schemes, the so-called combined rotation and multiple pulse sequence (CRAMPS) approach [20–23]. While MAS averages the chemical shift anisotropy, the RF must eliminate the dipolar interaction. Many RF decoupling schemes were developed through the years, starting with the off-resonance Lee–Goldburg (LG) RF irradiation [24] and the on-resonance multiple pulse scheme WAHUHA [25]. We have been using the phase modulated LG (PMLG*n*) experiment [26,27] to obtain 1D and 2D proton spectra. This method is based on the frequency modulated version of LG, FSLG (frequency switched LG [28]). The repeating RF unit of PMLG*n* consists of *2n* on-resonant RF pulses with discrete phase differences. Detection windows can be inserted between the pulses (*w*PMLG*n*) [29] allowing direct detection of the decoupled proton signal. Recently we have described the influence of RF phase and pulse imperfections on *w*PMLG*n* experiments and how they can be harnessed to improve the resultant proton spectra [30]. This scheme is named *w*PMLG*5**, to distinguish it from the ideal *w*PMLG*5* sequence. For certain RF offset values *w*PMLG*5** leads to effective spin rotations in the rotating frame around an axis approximately pointing in the *z* direction, hence resulting in the spectra devoid of images, providing higher signal-to-noise ratios and simplifying phase-cycling schemes [30].

The spectra of nuclei with spin quantum number larger than a half are broadened by the strong quadrupolar interaction, which can be of the order of several megahertz. Yet, for half-integer quadrupolar spins, the central transition (CT) is only affected by the quadrupolar interaction to a second order [31]. This broadening, though significantly smaller, cannot be averaged by MAS alone. Early line narrowing schemes were based on mechanical manipulations of the samples alone, either by combining two rotors (double rotation—DOR [32]), or by flipping the rotation axis of a single rotor between two orientations (dynamic angle spinning—DAS [33]). In 1995, Harwood and Frydman [16] showed that MQMAS can provide high-resolution spectra for half-integer quadrupolar spins by correlating different orders of symmetric spin coherences. Later Gan showed that correlation of satellite and symmetric coherences (STMAS) can also provide high-resolution spectra [17]. In MQMAS, the non-uniform excitation of the crystallites in the powder, either during creation of MQ coherences or during their conversion into 1Q coherences, causes lineshape distortions and signal attenuation. It has been shown that in addition to the introduction of higher spinning frequencies and higher RF powers, RF pulse shaping may provide a significant signal-to-noise increase. The introduction of fast amplitude modulation (FAM [34–36]) proved especially efficient, leading to 3- to 4-fold signal enhancements and better lineshapes in MQMAS.

Heteronuclear correlation (HETCOR) NMR experiments are commonly used for spectral editing and for the collection of structural constraints in both liquid and solid state NMR. HETCOR schemes correlating half-integer quadrupolar spins and spin-1/2 nuclei for pairs such as ^{23}Na–^{31}P [37] and ^{27}Al–^{31}P [38], have been already proposed and shown to be feasible. Spectral editing of quadrupolar spins based on their correlation to protons has so far been performed using CP editing of MQMAS spectra [39,40] and rotor-encoded MQMAS spectra [41]. An efficient CP coherence transfer between half integer quadrupolar spins and spins-1/2 can be expected at the Hartman–Hahn (HH) condition [12] modified for MAS [13] and adapted for a selective irradiation of the quadrupolar spin central transition [42]:

$$(S + 1/2)\nu_{1,Q} = \nu_{1,H} + n\nu_r, \quad (1)$$

where $\nu_{1,Q}$ is the RF intensity applied on the quadrupolar nucleus, ν_r is the spinning frequency, S is the spin quantum number of the quadrupolar nucleus and $\nu_{1,H}$ is the proton RF intensity. Cross polarization to or from quadrupolar nuclei is, however, a complicated process as was discussed comprehensively by Vega [42]. Since spin locking of the coherence of the central transition of a quadrupolar nucleus can only be obtained when the adiabatic transitions between the single- and multiple-quantum coherences are avoided [43], a low intensity RF irradiation field must be applied on the quadrupolar spin during the CP process. It has been shown recently that it is feasible to cross polarize higher order transitions of quadrupolar nuclei, using relatively high proton and aluminum RF fields, of the order of a 100 kHz [40].

In this paper, we demonstrate how half-integer quadrupolar spins and protons can be correlated in a high-resolution two-dimensional experiment and use this MQMAS-*w*PMLG scheme to establish Na–H correlations and assign the three Na^+ sites in sodium citrate dihydrate.

2. Results and discussion

2.1. The pulse sequence

The HETCOR pulse sequence utilized to obtain two-dimensional ^{23}Na–^{1}H correlation spectra, which is based on the one suggested by Wang et al. [37], is shown in Fig. 1. An amplitude modulated split-t1 MQMAS scheme was used to establish the ^{23}Na quadrupolar echo. Sensitivity enhancement was obtained by applying an FAM scheme [34]. At the echo position a CP mixing time transfers single quantum coherences from the

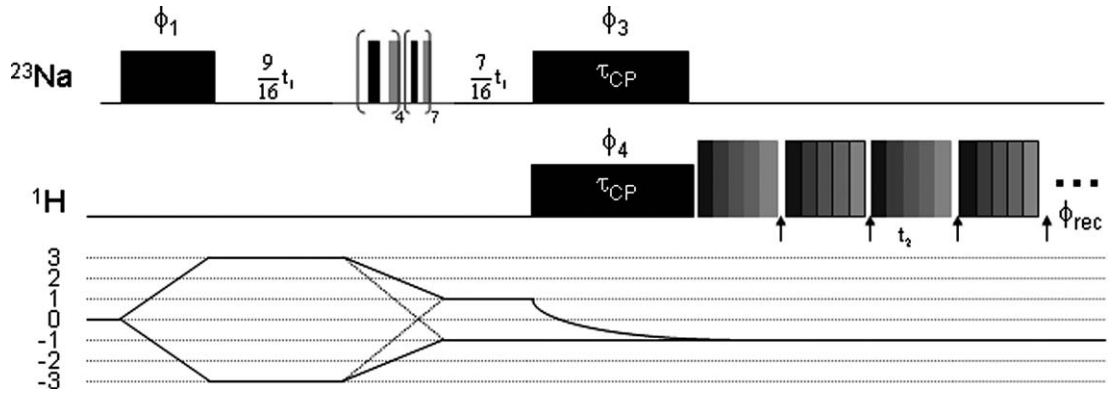

Fig. 1. The MQMAS-*w*PMLG pulse sequence for high-resolution HETCOR experiments between half-integer quadrupolar spins and protons. High-resolution in the quadrupolar spin dimension is obtained using an FAM-enhanced amplitude modulated split-t1 MQMAS scheme. Coherence transfer is achieved with a single-quantum cross polarization pulse at the MAS Hartmann–Hahn condition, modified for quadrupolar spins, $2\nu_{1,Q} = \nu_{1,H} - 2\nu_r$. High-resolution proton spectra is obtained with the image free windowed phase-modulated Lee–Goldburg scheme (*w*PMLG5*). The coherence pathway is indicated with a solid line. Acquisition points are indicated by the arrows in between PMLG pulses. The dotted line indicates a coherence pathway for 3QMAS on spins larger than 3/2. In general, cross-polarization from the echo signal of a spin S when initial $|p|$-quantum coherences are generated ($|p| = 3$ is shown in the example) is represented by the solid line for $|p| = 2S$, and should be modified according to the dotted line for the cases in which $|p| < 2S$. Depending on $|p|$ and S, the time delays $9t_1/16$ and $7t_1/16$, which are suitable to $|p| = 3$ and $S = 3/2$, should be modified to $t_1/(1 + |k|)$ and $|k|t_1/(1 + |k|)$, where $k = p\frac{36S(S+1)-17p^2-10}{36S(S+1)-27}$.

sodium atoms to nearby protons via their mutual dipolar couplings. Finally, a wPMGL5* [30] scheme was applied for the observation of high-resolution proton spectra.

2.2. CP optimization

For a ^{23}Na nucleus, $S = 3/2$, the HH condition of Eq. (1) becomes $\nu_{1,H} = 2\nu_{1,Na} + 2\nu_r$, with $n = -2$. To achieve an efficient transfer, the Na RF power level must be kept low to avoid adiabatic transfers between single- and multiple-quantum transitions. In addition, rotary resonance conditions at $(S + 1/2)\nu_{1,Na} = n\nu_r$ should be avoided in order not to quench the cross polarization process. These rotary resonances were observed during ^{27}Al–^{29}Si coherence transfer experiments on the mineral albite [51] and have also been shown to quench polarization transfer in FASTER-MQMAS [52] (In this method RF power is set in between rotary resonance conditions to obtain improved signal-to-noise). The latter effect has been discussed and explained using bimodal Floquet theory [53]. Finally, the upper limit of the spinning frequency (and thus the proton RF power) is determined by the *w*PMLG5 sequence, which requires ν_r values lower than about 20 kHz, and by the hardware performance, in our case 14–15 kHz.

Considering all these complications, we decided to perform numerical calculations, using the SIMPSON program [54], and to simulate the polarization transfer efficiency between the central transition of an $S = 3/2$ nucleus and a proton during cross-polarization. This was done by calculating the maximum intensity of the proton signal of an isolated sodium–proton spin pair in a powder sample after an excitation of the central transition of the sodium spin followed by CP mixing pulse. The results of these simulations are shown in Fig. 2. Using a nuclear quadrupolar coupling constant of 2.5 MHz and a proton RF intensity satisfying Eq. (1) with $n = -2$, the maximum proton signal intensities are drawn as a function of the ^{23}Na RF intensity and the spinning frequency. The results suggest the following: cross-polarization is indeed efficient only at low RF power levels (for $\nu_{1,Na} > 20$ kHz almost no intensity is observed); narrow rotary resonance conditions, satisfying $(S + 1/2)\nu_{1,Na} = n\nu_r$ and reducing the coherence transfer, should be avoided; the CP process is most efficient at spinning frequencies that are larger than 15–20 kHz. The small frame at the top shows an enlargement of the area corresponding to our experimental conditions. The relevant region is the crossing between the horizontal lines ($\nu_{1,Na} = 7$–8 kHz) and the vertical lines ($\nu_{RF} = 12.5$–13.5 kHz), obeying Eq. (1) for $\nu_{1,H} \sim 41$ kHz. In this range reasonable proton signal intensities can be expected. Although offset effects were not calculated, in our case an offset of the Na sites of $\sim$2 kHz is not expected to affect the Hartman–Hahn matching condition and therefore the CP efficiency. The contribution to the nutation frequency ($2\nu_{1,Na} = 15$ kHz) from an offset of 2 kHz is smaller than 150 Hz while the width of the HH condition is in the order of the size of the dipolar interaction, 250–1500 Hz in our case (see next paragraph). Thus we may safely say that offset effects are negligible in our experiment. As discussed above, working at higher spinning frequencies was not feasible due to hardware limitations and is not recommend because of the reduction in the *w*PMLG decoupling efficiency.

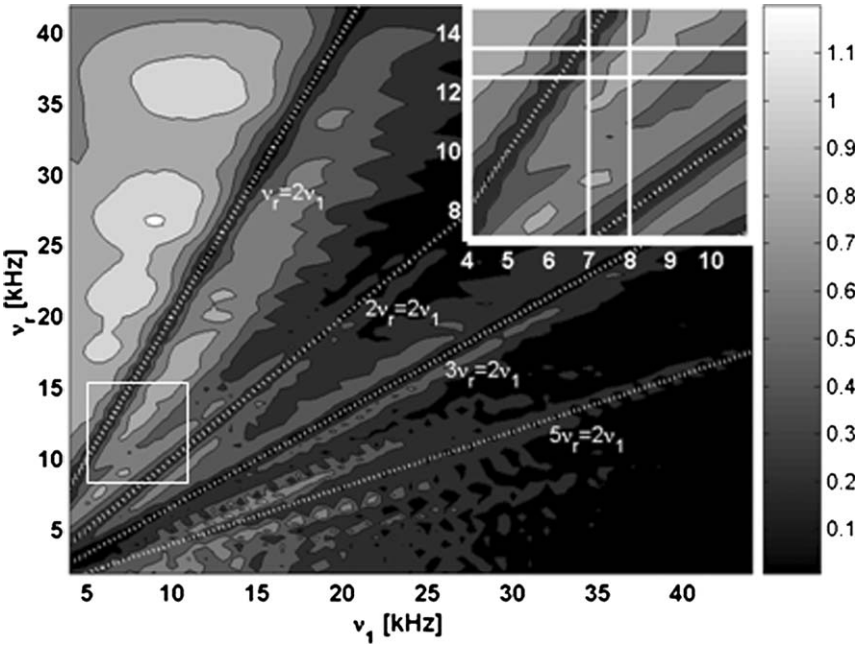

Fig. 2. Simulations of the cross polarization process between a single sodium spin and a single proton. The maximum intensity obtained in the CP process at each point in the ν_r/ν_{1Na} space is shown (relative to an ideal intensity of 4 of the central transition). A grid of 0.5 kHz in the RF level axis (ν_{1Na}) and 0.5 kHz in the spinning frequency axis (ν_r) was used. The ^{1}H RF intensity was set according to the MAS HH condition (Eq. (1)) with $n = -2$, for each point on the grid. The top right frame is a magnification of the region of interest, shown in white box. The area enclosed between the horizontal and vertical solid white lines was used in our experiments. Narrow rotary resonance regions are indicated with a broken white line for $n\nu_r = (S + 1/2)\nu_1$ for $n = 1, 2, 3$, and 5.

2.3. The HETCOR data

The 2D spectra obtained from the experiments on sodium citrate dihydrate are shown in Fig. 3. The left frame (Fig. 3A) presents the ^{23}Na MQMAS spectrum, showing three peaks that correspond to the three crystallographically inequivalent Na^+ cations in the asymmetric unit cell [44].

The results of the HETCOR experiments, performed with CP contact times of 1.25 and 0.4 ms, appear in Figs.

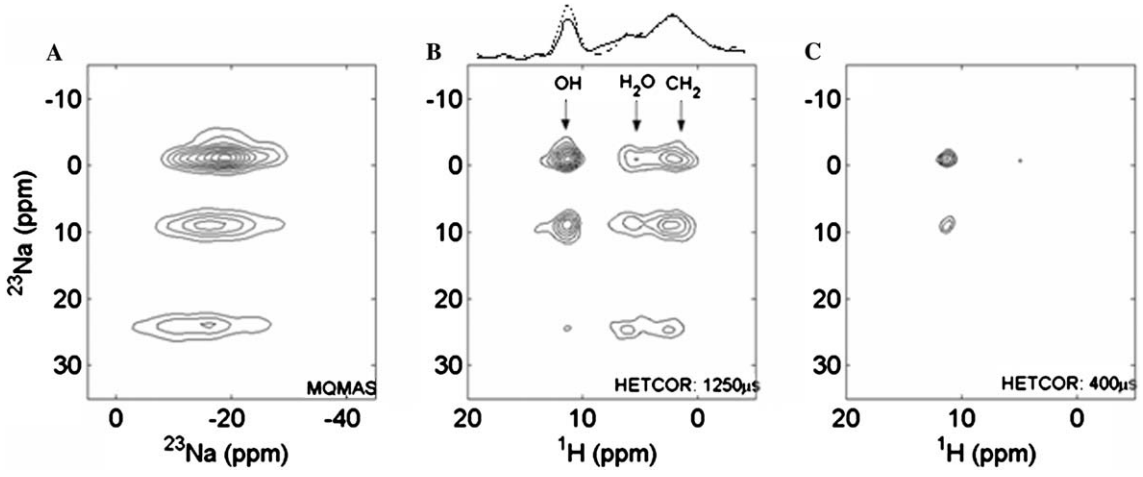

Fig. 3. Results of (A) a phase modulated, shifted echo, FAM-enhanced MQMAS experiment on sodium citrate dehydrate and (B) high-resolution ^{23}Na–^{1}H MQMAS-*w*PMLG HETCOR experiments with a CP contact time of 1.25 ms and (C) with a CP contact time of 0.4 ms, are shown. Contour levels in (A) appear at increments of 10% of the maximum intensity. Contour levels in (B) and (C) appear at increments of 10% of the maximum intensity in (B) with the minimum contour at 25%. On the top of spectrum (B) the sum projections along the ^{23}Na axis around −1 (dash line) and 9 (solid line) ppm are shown. In (A) the ^{23}Na axis was referenced to NaCl at 0 ppm and labeled in the isotropic indirect dimension according to the $C_{k(1)}$ convention, i.e. the spectral width corresponds to a dwell time consisting of multiple- and single-quantum evolution periods, the ppm scale is obtained by using an apparent carrier frequency similar to the ^{23}Na Larmor frequency, 79.39 MHz, and the chemical shift δ_{F1} is scaled according to $^{17}/_{8}\delta$, with $\delta_{NaCl} = 0$. This scaling was used for all three spectra. The proton positions in the spectra of OH, H_2O, and CH_2 are indicated by arrows in (B) and are similar in (C). The two H_2O molecules (labeled 8 and 9 in Fig. 4) and the two CH_2 groups (2 and 4) were unresolved in the spectrum.

3B and 3C, respectively. Three proton lines can be distinguished, corresponding to the protons of OH, H_2O, and CH_2 as indicated by the arrows. The *w*PMLG5* sequence resolved these three sites completely, while no spectral resolution was obtained in the proton MAS spectrum (not shown). The strongest cross peaks, corresponding to the closest sodium–proton contacts, appear in the spectra at the OH proton chemical shift. In Fig. 4, a single citrate ion, with its three sodium cations and two neighboring water molecules (corresponding to an asymmetric unit) is shown with the sodium–hydroxyl proton distances indicated by dashed lines. The shortest distances between the sodium atoms and the hydroxyl protons, deduced from the crystal structure data, are for Na(1) 5.18 and 4.97 Å (corresponding to dipolar couplings of 230 and 260 Hz), for Na(2) 2.89 and 3.55 Å (1330 and 715 Hz), and for Na(3) 2.75 and 3.79 Å (1540 and 590 Hz). Hence, we can expect that the strongest CP correlation peaks in the 2D spectra will appear between the OH protons and Na(2) and Na(3). Since in both spectra (3B) and (3C) strong cross peaks appear only for two sodium sites, we may safely deduce that the sodium at ~24 ppm, which we designate Na_{24}, corresponds to Na(1). Additional cross peaks correlating the H_2O (assigned in Fig. 4 by H8A–O8–H8B and H9A–O9–H9B) and CH_2 (C2–H2A–H2B and C4–H4A–H4B) protons to the sodium atoms Na(1–3) appear in Fig. 3B. To distinguish between Na(2) and Na(3), we compare the intensity ratio of these two sites in the MQMAS and in the HETCOR experiments. A ratio between the sodium peaks Na_{-1}:Na_9 of 1.7:1 was obtained by calculating the integrated intensity of the corresponding two-dimensional MQMAS peaks. To evaluate the relative sodium line intensities after cross-polarization proton spectra were calculated by summing separately the Na_{-1}–H and Na_9–H slices along the Na dimension in the HETCOR spectrum of Fig. 3B. A Na_{-1}:Na_9 ratio can then be obtained for each type of protons by measuring proton line intensities. This ratio equals to 1:1 for the CH_2 protons. This can be seen in the spectra drawn on top of Fig. 3B, where the CH_2 lines corresponding to Na_{-1} (dash line) and Na_9 (solid line) are apparently similar. Combining the two ratios (from MQMAS and from HETCOR) shows that for a mixing time of 1.25 ms the Na_9–CH_2 CP efficiency is almost twice as large as the Na_{-1}–CH_2 efficiency. An examination of the sodium to CH_2–protons distances gives for Na(3)–H4A/B distances of 3.3/3.6 Å and for Na(2)–H2A/B distances of

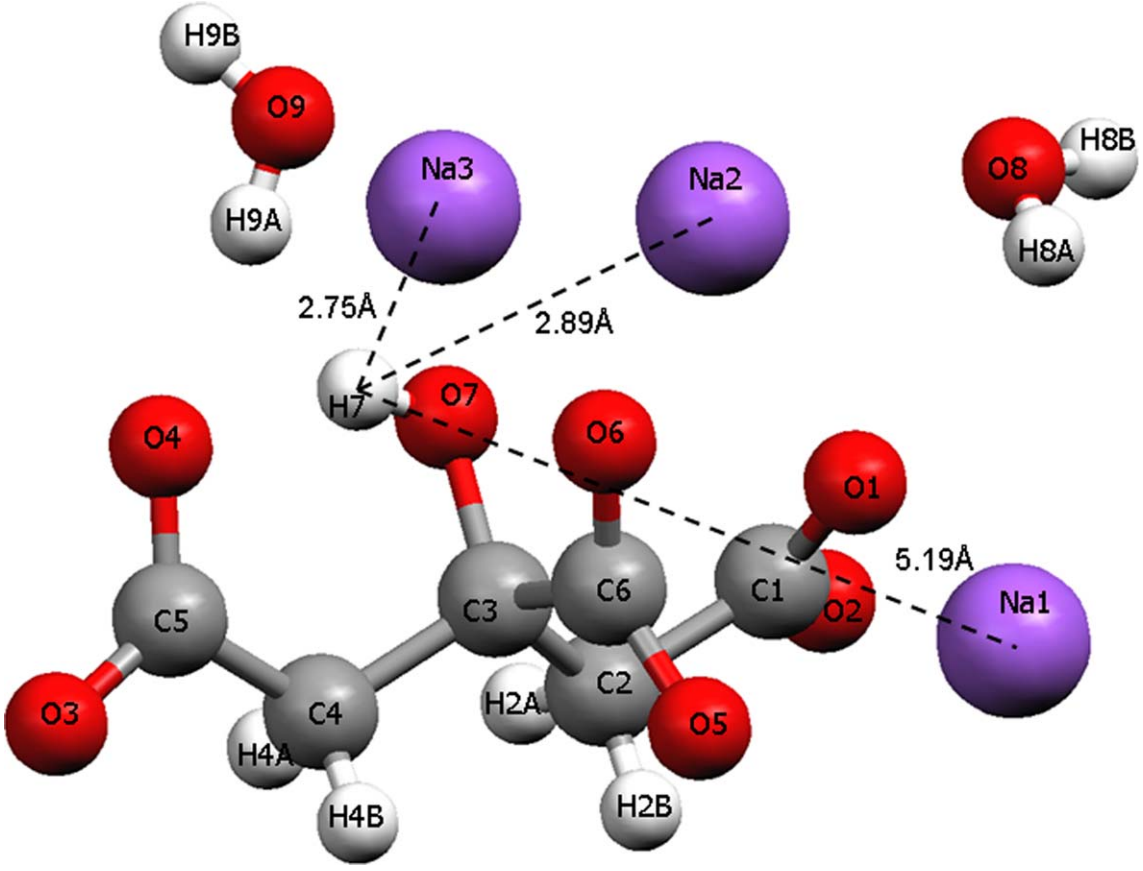

Fig. 4. The asymmetric unit of a sodium citrate dihydrate, $3Na^+ \cdot C_6H_5O_7^{3-} \cdot 2H_2O$ [44]. Intra-molecular Na(1–3)–H7 distances are indicated by dotted lines, with their corresponding distances. The plot and the distance calculations were obtained using the Mercury software [55].

4.2/4.5 Å. These distances correspond to dipolar interactions of strength 0.79 ± 0.1 kHz and 0.39 ± 0.04 kHz, respectively, and we can assign Na(3) to Na_9.

This assignment can be further certified by examining the cross peak intensities between Na_{-1} and Na_9 and the H7 hydroxyl protons. From the proton spectra in Fig. 3B it follows that the Na_{-1}:Na_9 intensity ratio at the OH-positions in the HETCOR spectrum equals 1.3:1. Together with the MQMAS sodium ratio the CP efficiency ratio becomes 0.76:1 and again Na_9 shows a somewhat stronger interaction and thus a shorter distance. From the crystal structure it follows that the shortest sodium to OH–proton distances are for Na(2) 2.89 Å (corresponding to 1.33 kHz) and for Na(3) 2.75 (corresponding to 1.53 kHz). This again indicates that Na(3) resonates at 9 ppm.

To validate that the difference in intensities does not arise from differences in CP efficiencies due to the different quadrupolar interaction strengths of the sodium nuclei, $\chi = 1.65$ MHz for Na_9 and $\chi = 1.1$ MHz for Na_{-1} [34], we have calculated CP transfer curves of single spin pairs ^{23}Na(central transition)–^{1}H for χ values between 1 and 2 MHz. Assuming RF intensities as well as a spinning frequency as in our experiments, non-significant differences during the proton-signal build-up were detected up to ~1.3 ms.

Another observation is the reduced efficiency of the CP transfer to the water molecules. Although several of the water protons are located at distances of 2.5 Å (Na(3)–H9A), 2.8 Å (Na(1)–H8A/H8B), and 2.9Å (Na(2)–H8A/H8B), approximately the same distance as the hydroxyl protons, they all have lower cross peak intensities. This reduction in CP efficiency presumably is due to exchange motions of the water molecules in the crystal.

3. Experimental

3.1. The sample

Experiments were performed on sodium citrate dihydrate, $3Na^+ \cdot C_6H_5O_7^{3-} \cdot 2H_2O$. This crystalline material is monoclinic and has the space group $C2/c$. Its crystal structure was determined recently and the coordinates of all atoms in the unit cell were listed [44]. The hydrogen atoms were positioned in the structure by refining it, starting with C–H distances equal to 0.97 Å and O–H and H–H distances in water of 0.82 and 1.32 Å, respectively.

3.2. NMR

Data were acquired on a Bruker DSX300 spectrometer with a TR WB 4 mm MAS probe. The Larmor frequencies were 300.13 and 79.39 MHz for ^{1}H and ^{23}Na, respectively.

3.3. 2D MQMAS

All parameters of our split-t1 shifted-echo MQMAS experiment [45], together with the phase cycling scheme, are summarized in the tables below.

The pulse sequence parameters:

Acquisition points	128×512
Spectral points	512×1024
Number of scans	96
Dwell times ($t_1 \times t_2$)	$38.5\,\mu \times 10\,\mu$
Relaxation delay	5 s
Spinning frequency	13 kHz
$\nu_{1,Na}$ (during MQMAS)	86 kHz
3Q-excitation pulse length	7 μs
3Q → SQ FAM conversion	F_4^I (4.4 μs)F_7^I (2.4 μs) [46]
Echo delay (τ_{echo})	2 ms
Selective π echo pulse length	12 μ

Phase cycling:

3Q excitation	0,30,60,90,120,150,180,210,240, 270,300,330
FAM pulses	0
Echo pulse	0_{12}, 45_{12}, 90_{12}, 135_{12}, 180_{12}, 225_{12}, 270_{12}, 315_{12}
Receiver phase	$[0\ 270\ 180\ 90]_3$, $[90\ 0\ 270\ 180]_3$, $[180\ 90\ 0\ 270]_3$, $[270\ 180\ 90\ 0]_3$

3.4. MQMAS-wPMLG HETCOR

The HETCOR sequence was derived according to Wang et al. [37]. The proton MAS acquisition was replaced by the *w*PMLG5* scheme. All parameters defining our 2D HETCOR experiments, shown in Fig. 1, are listed here below

The time periods

The quadrupolar evolution	Amplitude-modulated split-t1 MQMAS
The mixing time	Single-quantum cross polarization
The proton detection	*w*PMLG5*

The pulse sequence parameters:

Acquisition points	64×512
Spectral points	1024×2048
Scans	96
Dwell times ($t_1 \times t_2$)	$77\,\mu \times 24.4\,\mu$
Relaxation delay	5 s
Spinning frequency	13 kHz
3Q-excitation pulse length	7 μs

$3Q \rightarrow SQ$ FAM conversion	$F_4^I(4.4\,\mu s)F_7^I(2.4\,\mu s)$
$\nu_{1,Na}$ (MQMAS)	86 kHz
$\nu_{1,Na}$ (during CP)	7.5 kHz
$\nu_{1,H}$ (during CP)	41 kHz
PMLG5 phase increments	$\pm 41.6°$
Initial phase, positive direction	20.78°
Initial phase, negative direction	7.02°
Length of phase single pulse	1.74 μ
Length of detection window (t_w)	7 μ
$\nu_{1,h}$ (during *w*PMLG5*)	82 kHz
Preamplifier filter width (max)	10^9 Hz
Phase sensitive detection	TPPI (on ϕ_3) [47]

Phase cycling according to Fig. 1:

ϕ_1	0,60,120,180,240,300
ϕ_2	0
ϕ_3	0_6, 90_6, 180_6, 270_6
ϕ_4	0_{24}, 90_{24}, 180_{24}, 270_{24}
ϕ_{rec}	$\{[0,180]_3, [180,0]_3\}_2$, $\{[90,270]_3, [270,90]_3\}_2$, $\{[180,0]_3, [0,180]_3\}_2$, $\{[270,90]_3, [90,270]_3\}_2$

Data processing was done offline using the matNMR program[48]. MQMAS data was processed according to [45]: data points were shifted with respect to the echo center ensuring FT spectra devoid of imaginary contributions in F2, thus providing pure absorption lineshapes.

The ^{23}Na isotropic axis was labeled according to the $C_{k(1)}$ convention [49]: the chemical shift positions were referenced to $(k-p)/(1+k)\delta_{NaCl} = 17/8\delta_{NaCl}$ for spin-3/2 with $k = 7/9$ the MQMAS ratio and $p = -3$ the coherence order for the echo pathway.

3.5. Nuclei with $S > 3/2$

It is worthwhile noticing that the 2D HETCOR experiment can also be extended to nuclei with spins larger than 3/2. In that case the pulse sequence should be adjusted. To obtain a particular *p*QMAS spectrum in the F_1-dimension from a nucleus with spin quantum number S with a multiple-quantum coherence order $|p|$ smaller than $2S$, a coherence pathway $\pm p \rightarrow \mp 1 \rightarrow -1$ should be chosen, so that ϕ_1 is phase cycled with a basic step of $360°/2p$ and the receiver phase is modified according to [47], $\phi_{rec} = -\sum_i \Delta p_i \phi_i$ (dotted line in the coherence pathway diagram, Fig. 1). Otherwise, when $p = 2S$, the pathway $\pm p \rightarrow \pm 1 \rightarrow -1$ is to be picked, again by adjusting ϕ_1 and ϕ_{rec}. A suitable choice of the MQMAS RF shaping pulses must be made in order to achieve better sensitivity [50].

4. Conclusions

In this paper, we have shown a method to obtain high-resolution 2D HETCOR spectra of half-integer quadrupolar spins coupled to protons. High-resolution spectra are obtained by correlating a split-t1 MQMAS scheme in the indirect dimension with a *w*PMLG5* proton detection scheme. Transfer of coherence is achieved via standard cross-polarization. By recording spectra at several contact times, qualitative information regarding proximity of the atoms can be obtained. This technique allowed us to assign the three Na^+ sites in sodium citrate dihydrate. Improved selectivity may be obtained by using Lee–Goldburg cross polarization or any other qualitative scheme. This experiment provides an additional tool for the spectral editing of protons and some interesting half-integer quadrupolar spins such as ^{23}Na, ^{17}O, ^{27}Al, ^{67}Zn, and ^{25}Mg. The experiment may be easily adjusted to nuclei with spins 5/2 and larger by a modification of its coherence pathway and phase cycling scheme.

Acknowledgments

This research was supported by the Minerva Science Foundation. We wish to thank P.K. Madhu for his assistance in setting up the 2D HETCOR experiments.

References

[1] K. Schmidt-Rohr, H.W. Spiess, Multidimensional Solid State NMR and Polymers, Academic Press, London, 1994.
[2] F. Castellani, B. van Rossum, A. Diehl, M. Schubert, K. Rehbein, H. Oschkinat, Structure of a protein determined by solid-state magic-angle-spinning NMR spectroscopy, Nature 420 (2002) 98–102.
[3] R. Tycko, Applications of solid state NMR to the structural characterization of amyloid fibrils: methods and results, Prog. NMR Spectr. 42 (2003) 53–68.
[4] Thompson, K. Lynmarie, Solid-state NMR studies of the structure and mechanisms of proteins, Curr. Opin. Struct. Bio. 12 (2002) 661–669.
[5] A.E. McDermott, A. Bockmann, Assignments and prospects for sructure determination of solid proteins Using MAS and isotopic enrichment, in: Encyclopedia of NMR, Suppl. 9, Wiley, Chichester, 2002.
[6] M.H. Cohen, F. Reif, in: Quadrupole Effects in Nuclear Magnetic Resonance Studies of Solids, Solid State Physics, vol. 5, Academic Press, New York, 1957.
[7] E.R. Andrew, A. Bradbury, R.G. Eads, Nuclear magnetic resonance spectra from a crystal rotated at high speed, Nature 182 (1958) 1659.
[8] I.J. Lowe, Free induction decays of rotating solids, Phys. Rev. Lett. 2 (1959) 285–287.

[9] V. Royden, Measurement of the spin and gyromagnetic ratio of C^{13} by the collapse of spin–spin splitting, Phys. Rev. 96 (1954) 543–544.
[10] A.L. Bloom, J.N. Shoolerly, Effects of perturbing radiofrequency fields on nuclear spin coupling, Phys. Rev. 97 (1955) 1261–1265.
[11] M. Mehring, A. Pines, W.K. Rhim, J.S. Waugh, Spin-decoupling in the resolution of chemical shifts in solids by pulsed NMR, J. Chem. Phys. 54 (1971) 3239–3240.
[12] S.R. Hartmann, E.L. Hahn, Nuclear double resonance in the rotating frame, Phys. Rev. 128 (1962) 2042–2053.
[13] A. Pines, M.G. Gibby, J.S. Waugh, Proton-enhanced NMR of dilute spins in solids, J. Chem. Phys. 59 (1973) 569–590.
[14] E.O. Stejskal, J. Schaefer, J.S. Waugh, Magic-angle spinning and polarization transfer in proton-enhanced NMR, J. Magn. Reson. 28 (1977) 105–112.
[15] U. Haeberlen, High resolution NMR in solids. Selective averaging, in: Advances in Magnetic Resonance Suppl. 1, Academic Press, 1975.
[16] L. Frydman, J.S. Harwood, Isotropic spectra of half-integer quadrupolar spins from bidimensional magic-angle spinning NMR, J. Am. Chem. Soc. 117 (1995) 5367–5368.
[17] Z. Gan, Isotropic NMR spectra of half-integer quadrupolar nuclei using satellite transitions and magic-angle spinning, J. Am. Chem. Soc. 122 (2000) 3242–3243.
[18] M. Mehring, in: High Resolution NMR Spectroscopy in Solids, NMR, Basic Principles and Progress, vol. 11, Springer, Germany, 1976.
[19] B.C. Gerstein, C. Clor, R.G. Pembleton, R.C. Wilson, Utility of pulse nuclear magnetic resonance in studying protons in coals, J. Phys. Chem. 81 (1977) 565–570.
[20] C.E. Bronnimann, B.L. Hawkins, M. Zhang, G.E. Maciel, Combined rotation and multiple pulse spectroscopy as an analytical proton nuclear magnetic resonance technique for solids, Anal. Chem. 60 (1988) 1743–1750.
[21] M.L. Buszko, C.E. Bronnimann, G.E. Maciel, ^{1}H CRAMPS based on TREV, J. Magn. Reson. Ser. A 103 (1993) 183–187.
[22] U. Haeberlen, J.S. Waugh, Coherent averaging effects in magnetic resonance, Phys. Rev. 175 (1968) 453–467.
[23] M. Lee, W. Goldburg, Nuclear magnetic resonance line narrowing by rotating rf fields, Phys. Rev. 140 (1965) A1261–A1271.
[24] J.S. Waugh, L.M. Huber, U. Haeberlen, Approach to high resolution NMR in solids, Phys. Rev. Lett. 20 (1968) 180–182.
[25] M. Mehring, J.S. Waugh, Magic-angle NMR experiments in solids, Phys. Rev. B 5 (1972) 3459–3471.
[26] E. Vinogradov, P.K. Madhu, S. Vega, High-resolution proton solid state NMR spectroscopy by phase-modulated Lee–Goldburg experiment, Chem. Phys. Lett. 314 (1999) 443–450.
[27] E. Vinogradov, P.K. Madhu, S. Vega, A bimodal Floquet analysis of phase modulated Lee–Goldburg high resolution proton magic angle spinning NMR experiments, Chem. Phys. Lett. 329 (2000) 207–214.
[28] M.H. Levitt, A.C. Kolbert, A. Bielecki, D.J. Ruben, Proton line-narrowing in solids with frequency-switched pulse sequences, Solid State Nucl. Magn. Reson. 2 (1993) 151–163.
[29] E. Vinogradov, P.K. Madhu, S. Vega, Proton spectroscopy in solid state nuclear magnetic resonance with windowed phase modulated Lee–Goldburg decoupling schemes, Chem. Phys. Lett. 354 (2002) 193–202.
[30] L. Bosman, P.K. Madhu, S. Vega, E. Vinogradov, Radio frequency imperfections in windowed phase modulated Lee–Goldburg decoupliong experiments, J. Magn. Reson. (in press).
[31] D. Freude, Quadrupolar nuclei in solid-state nuclear magnetic resonance, in: R.A. Meyers (Ed.), Encyclopedia of Analytical Chemistry, Wiley, Chichester, 2000, pp. 12188–12224.
[32] A. Samoson, E. Lippmaa, A. Pines, High resolution solid-state NMR averaging of 2nd-order effects by means of a double-rotor, Mol. Phys. 65 (1988) 1013–1018.
[33] A. Llor, J. Virlet, Towards high-resolution NMR of more nuclei in solids: sample spinning with time-dependent spinner axis angle, Chem. Phys. Lett. 152 (1988) 248–253.
[34] P.K. Madhu, A. Goldbourt, L. Frydman, S. Vega, Fast radiofrequency amplitude modulation in multiple-quantum magic-angle spinning nuclear magnetic resonance: theory and experiments, J. Chem. Phys. 112 (2000) 2377–2391.
[35] A. Goldbourt, P.K. Madhu, S. Vega, Enhanced conversion of triple to single-quantum coherence in the triple-quantum MAS NMR spectroscopy of spin-5/2 nuclei, Chem. Phys. Lett. 320 (2000) 448–456.
[36] A. Goldbourt, P.K. Madhu, S. Kababya, S. Vega, The influence of the radiofrequency excitation and conversion pulses on the intensities and lineshapes of the triple-quantum MAS NMR spectra of $I = 3/2$ nuclei, Solid State Nucl. Magn. Reson. 18 (2000) 1–16.
[37] S.H. Wang, S.M. De Paul, L.M. Bull, high-resolution heteronuclear correlation between quadrupolar and spin-$\frac{1}{2}$ nuclei using multiple-quantum magic-angle spinning, J. Magn. Reson. 125 (1997) 364–368.
[38] C. Fernandez, L. Delevoye, J.-P. Amoureux, D.P. Lang, M. Pruski, High-resolution heteronuclear correlation spectra between ^{31}P and ^{27}Al in microporous aluminophosphates, Solid State Nucl. Magn. Reson. 21 (2002) 61–70.
[39] C. Fernandez, L. Delevoye, J.-P. Amoureux, D.P. Lang, M. Pruski, ^{27}Al{^{1}H} Cross Polarization Triple-Quantum Magic Angle Spinning NMR, J. Am. Chem. Soc. 119 (1997) 6858–6862.
[40] S.E. Ashbrook, S.P. Brown, S. Wimperis, Multiple-quantum cross-polarization in MAS NMR of quadrupolar nuclei, Chem. Phys. Lett. 288 (1998) 509–517.
[41] A. Lupulescu, S.P. Brown, H.W. Spiess, Rotor-encoded heteronuclear MQ MAS NMR spectroscopy of half-iInteger quadrupolar and spin $I = 1/2$ nuclei, J. Magn. Reson. 154 (2002) 101–129.
[42] A.J. Vega, CP/MAS of quadrupolar $S = 3/2$ nuclei, Solid State Nucl. Magn. Reson. 1 (1992) 17–32.
[43] A.J. Vega, MAS NMR spin locking of half-integer quadrupolar nuclei, J. Magn. Reson. 96 (1992) 50–68.
[44] A. Fischer, G. Palladino, Trisodium citrate dihydrate, Acta Cryst. E 59 (2003) m1080–m1082.
[45] S.P. Brown, S. Wimperis, Two-dimensional multiple-quantum MAS NMR of quadrupolar nuclei. Acquisition of the whole echo, J. Magn. Reson. 124 (1997) 279–285.
[46] P.K. Madhu, O.G. Johannessen, K.J. Pike, R. Dupree, M.E. Smith, M.H. Levitt, Application of amplitude-modulated radio-frequency fields to the magic-angle spinning NMR of spin-7/2 nuclei, J. Magn. Reson. 163 (2003) 310–317.
[47] R.R. Ernst, G. Bodenhausen, A. Wokaun, Principles of Nuclear Magnetic Resonance in One and Two Dimensions, Clarendon Press, Oxford, 1987.
[48] MatNMR is a toolbox for processing NMR/EPR data under MATLAB and can be freely downloaded at http://matnmr.sourceforge.net.
[49] Y. Millot, P.P. Man, Procedures for labeling the high-resolution axis of two-dimensional MQ-MAS NMR spectra of half-integer quadrupole spins, Solid State Nucl. Magn. Reson. 21 (2002) 21–43.
[50] A. Goldbourt, P.K. Madhu, Multiple-quantum magic-angle spinning: high-resolution solid-state NMR spectroscopy of half-integer quadrupolar nuclei, Monatshefte für Chemie 133 (2002) 1497–1534.

[51] S.M. De Paul, M. Ernst, J.S. Shore, J.F. Stebbins, A. Pines, J. Phys. Chem. B 101 (1997) 3240–3249.
[52] T. Vosegaard, P. Florian, D. Massiot, Multiple quantum magic-angle spinning using rotary resonance excitation, J. Chem. Phys. 114 (2001) 4618–4624.
[53] J.D. Walls, K.H. Lim, A. Pines, Theoretical studies of the spin dynamics of quadrupolar nuclei at rotational resonance conditions, J. Chem. Phys. 116 (2002) 79–90.
[54] M. Bak, J.T. Rasmussen, N.C. Nielsen, SIMPSON: a general simulation program for solid-state NMR spectroscopy, J. Magn. Reson. 147 (2000) 296–330.
[55] I.J. Bruno, J.C. Cole, P.R. Edgington, M. Kessler, C.F. Macrae, P. McCabe, J. Pearson, R. Taylor, New software for searching the Cambridge Structural Database and visualizing crystal structures, Acta Crystallogr. B 58 (2002) 389–397.